Photovoltaic characterization of concentrator solar cells by localized irradiation

Cite as: J. Appl. Phys. **100**, 044514 (2006); https://doi.org/10.1063/1.2266161
Submitted: 28 February 2006 • Accepted: 30 May 2006 • Published Online: 31 August 2006

Eugene A. Katz, Jeffrey M. Gordon, Wondesen Tassew, et al.

Photovoltaic characterization of concentrator solar cells by localized irradiation

Eugene A. Katz,[a] Jeffrey M. Gordon,[b] Wondesen Tassew, and Daniel Feuermann
Department of Solar Energy and Environmental Physics, Jacob Blaustein Institutes for Desert Research, Ben-Gurion University of the Negev, Sede Boqer Campus 84990, Israel

(Received 28 February 2006; accepted 30 May 2006; published online 31 August 2006)

The ability to determine the macroscopic parameters that characterize photovoltaic performance, including their spatial dependence, especially at high flux, is demonstrated with extensive solar measurements on high-efficiency concentrator solar cells. Two case studies explore (a) the impact of inhomogeneous flux distribution on photovoltaic behavior, (b) establishing how solar cell parameters vary across the cell surface (of particular interest for deployment in high-concentration optical systems), and (c), the sensitivity of photovoltaic parameters to the spatial variation of series resistance that stems from nonuniform cell metallization. In the process, we elucidate current-voltage trends unique to strongly inhomogeneous illumination and to series resistance losses at high flux. © *2006 American Institute of Physics*. [DOI: 10.1063/1.2266161]

I. INTRODUCTION

Recent advances in high-efficiency concentrator photovoltaic (PV) cells[1–3] prompt the need for performance studies at elevated solar concentration with particular attention to the sensitivity to flux distribution. Conversion efficiencies approaching 40%, attained only at flux levels of several hundred suns or greater, have been realized in III-V multijunction solar cells[1–3] (1 sun $\equiv$ 1 mW/mm^2). Practical compact miniaturized optics[1,4–6] can realize net flux values in excess of 10^3 suns at high collection efficiency and accommodate completely passive heat rejection with cell areas in the range of 1–100 mm^2. In earlier PV systems, concern over nonuniform illumination related to series-connected solar cells receiving different flux levels. Here, in contrast, we address flux inhomogeneities on a single cell, commensurate with the one-concentrator-one-cell strategy that has evolved in optically efficient, pragmatic, high-flux optics for concentrator PV cells.[1,4–6]

Few data have been published on the behavior of concentrator cells at high flux (hundreds to thousands of suns), with even less on the sensitivity to flux distribution and the spatial variations in PV parameters. These issues are germane for two reasons: (1) high-flux optics can generate strongly nonuniform intensity distributions on the cell[1,4,6] and (2) PV manufacturers need noninvasive techniques that can reveal where heightened resistance may arise.

We report how a localized irradiation (LI) procedure—based on a solar fiber-optic minidish concentrator[7–9]—was applied to two case studies. One examines unique aspects of how PV current-voltage (*I-V*) curves change under localized irradiation and appraises the uniform metallization grid. The other focuses on a cell with irregular metallization and provides a quality check of how PV parameters vary across the cell surface. Both instances effectively scrutinize the local effects of the cell's series resistance. The macroscopic LI method portrayed here relates to measuring inhomogeneities in PV performance on a millimeter scale, rather than more sophisticated focused-laser techniques for the detection of micron-scale defects. However, LI tests with laser light are problematic because (1) multijunction cells are acutely sensitive to current matching among the subcells, which would be severely compromised with monochromatic input, and (2) even multiple lasers specially tuned to satisfy current matching would deviate markedly from the solar spectrum and would render the results of questionable value.

II. EXPERIMENTAL DETAILS

A. Solar test facility

Our test facility (Fig. 1) comprises a dual-axis tracking minidish solar concentrator with a transmissive optical fiber

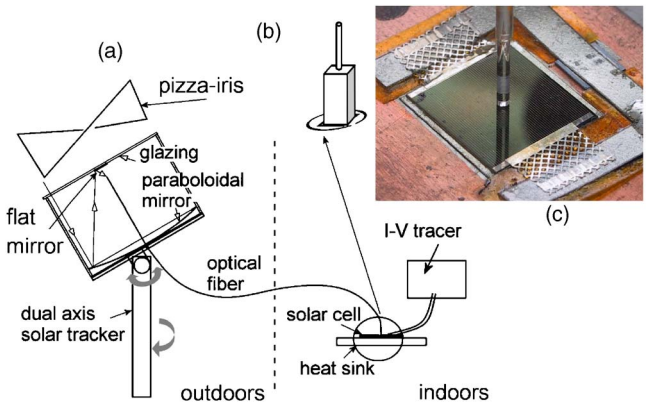

FIG. 1. (Color online) (a) Minidish solar concentrator (20 cm in diameter). The sun is imaged into the upward-facing tip of an optical fiber, which guides concentrated sunlight to an indoor laboratory where solar cell *I-V* curves are measured. Input power is moderated by a pizza-slice iris that preserves the angular distribution of delivered sunlight. (b) Uniform cell irradiation via a kaleidoscope. (c) Fiber-cell contact in the LI mode.

[a]Also at: The Ilse Katz Center for Meso and Nanoscale Science and Technology, Ben-Gurion University of the Negev, Beersheva 84105, Israel.
[b]Author to whom correspondence should be addressed; also at: The Pearlstone Center for Aeronautical Engineering Studies, Department of Mechanical Engineering, Ben-Gurion University of the Negev, Beersheva 84105, Israel; electronic mail: jeff@bgu.ac.il

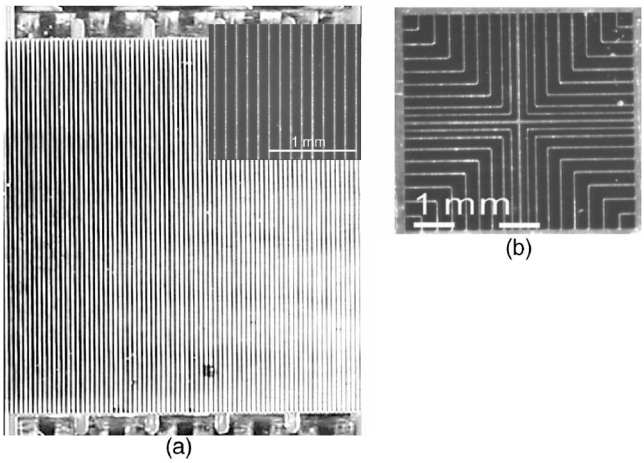

FIG. 2. Solar cells studied. (a) Square 100 mm^2 with a uniform grid. The inset magnifies the uniform metallization. (b) Square 30.25 mm^2 with a nonuniform grid.

1.0 mm in diameter channeling concentrated sunlight to an indoor test bench. LI refers to the fiber touching the cell such that radiation is confined to the circle delimited by the fiber tip [Figs. 1(a) and 1(c)]. *I-V* curves were measured as the fiber was moved across the cell surface. Near-perfect flux uniformity can be achieved with a square cross-section kaleidoscope that matches the size of the cell, placed between the distal fiber tip and the cell [Fig. 1(b)].[7] All physical and spectral characteristics were reported previously.[7] Net solar irradiation on the cell P_{in} was measured with a spectrum-blind pyrometer and moderated with an iris from 0.1 to 8 *W* [Fig. 1(a)]. The latter value corresponds to a LI flux of 10 200 suns. All measurements were performed during clear-sky periods, 2 h about solar noon, over the course of several months in Sede Boqer, Israel. The spectrum of light delivered to the cell was nearly invariant and close to the air mass 1.5 direct beam solar spectrum.[7]

B. Solar cells studied

We tested two types of commercial square triple-junction $GaInP_2/GaAs/Ge$ cells of the same nominal architecture,[2] differing only in their size and metallization grid: (1) 100 mm^2 cells with two bus bars and uniform front metallization [Figs. 1(c) and 2(a)] where the contact grid's parallel strips of equal thickness are spaced ~125 μm apart and (2) 30.25 mm^2 cells with four bus bars and a nonuniform front metallization of central symmetry where the distance between contact fingers varies from a minimum of ~190 μm at the center to a maximum of ~380 μm near the corners [Fig. 2(b)]. Each cell was thermally bonded to a passive copper heat sink that kept measured cell temperatures within 10 K of the indoor ambient temperature of 297 K.

III. EXPERIMENTAL RESULTS

A. Uniform grid cells

I-V curves were measured over a range of P_{in} for both (a) uniform illumination and (b) seven LI sites across the cell (Fig. 3, with the illuminated fraction f being 0.007 85). In all

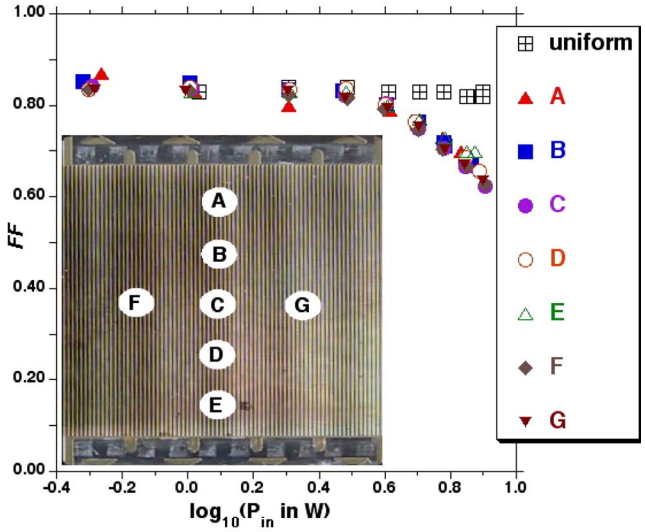

FIG. 3. (Color online) FF for the uniform grid cell measured under uniform irradiation and with LI at the seven indicated locations, with an experimental uncertainty in FF of 4% (relative).

instances, short-circuit current I_{sc} was proportional to P_{in} with a photocurrent generation ratio $G=I_{sc}/P_{in}=0.130\pm0.002$ A/W, independent of P_{in}.

Fill factor FF is a particularly sensitive indicator of series resistance losses [$FF=P_{max}/(I_{sc}V_{oc})$, where P_{max} denotes maximum power output and V_{oc} open-circuit voltage]. The fact that the same FF is measured at all seven LI sites, over the full range of P_{in} values (Fig. 3), attests to (1) the homogeneous spatial distribution of internal losses as well as (2) the negligible contribution of the front contact grid to the cell's series resistance[10] (at least for our LI conditions).

Figure 4 illustrates the influence of flux level and distribution on (a) V_{oc} and (b) efficiency $\eta=P_{max}/P_{in}$. The largest P_{in} value corresponds to a LI flux of $\sim10^4$ suns, yet produces a concentration of only ~75 suns when uniformly distributed over the entire cell with a kaleidoscope (well below the reported value of ~350 suns at which efficiency peaks[2]).

Representative *I-V* curves measured under uniform and localized irradiation are graphed in Fig. 5. Although flux distribution—varied from uniform to highly localized—has an indiscernible effect at lower P_{in} values, there is a pronounced degradation of the *I-V* curve at the higher P_{in} values. In Fig. 5(b), note the current drop at intermediate voltages (in the vicinity of 2.4 V) for all *I-V* curves recorded under LI at $P_{in}>5$ *W*—a feature absent in uniformly irradiated cells over the full range of P_{in} [Fig. 5(a)]. The reasons for the prominent differences in PV parameters between uniform and localized illumination will be addressed in Sec. IV.

B. Nonuniform grid cells

The nonuniform metallization may introduce a lateral dependence to the cell reflectivity as well as to the emitter contribution to the series resistance,[11,12] which can give rise to a corresponding lateral dependence for the principal PV indicators. The objective here is the elucidation of these nonuniformities by the LI method, not an assessment of whether inverted-square metallization can offer a lower effective se-

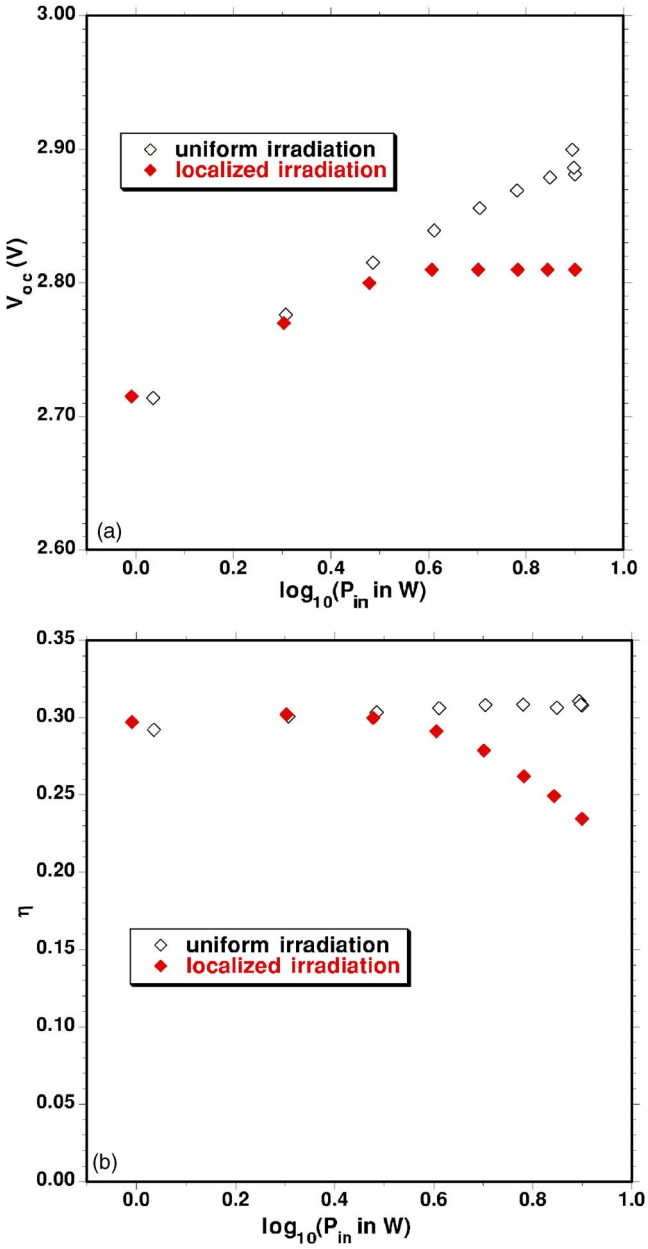

FIG. 4. (Color online) Dependence of V_{oc} and η on P_{in} for uniform and localized irradiation. The experimental uncertainties are 1% for V_{oc} and 5% (relative) for η.

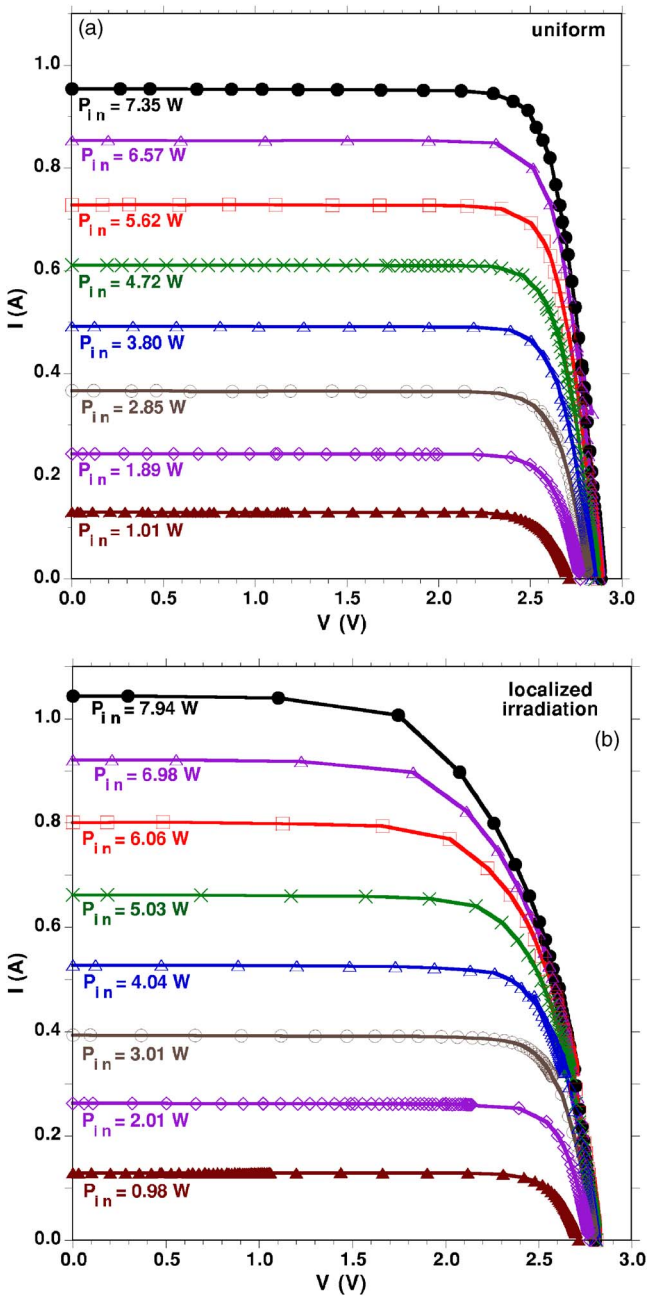

FIG. 5. (Color online) Representative *I-V* curves of the uniform grid cell measured under (a) uniform and (b) localized irradiation. The experimental uncertainty in both *I* and *V* is 1%.

ries resistance than its parallel-strip counterpart (it can, in part owing to superior electron channeling and in part due to the exploitation of four rather than two bus bars[12,13]). Namely, any observed performance inferiority of the irregular grid cells arises from the weakness of a specific metallization design (e.g., excessive spacing among fingers) rather than representing an intrinsic shortcoming.

Cell reflectivity, and hence G [the slope in Fig. 6(a)], depends on surface position as a consequence of the nonuniform distribution and width of the metal fingers. There is also a deviation in the proportionality of I_{sc} with P_{in} at the highest flux values for regions of less metallization [Fig. 6(a)]: a series resistance effect addressed in Sec. IV.

I-V curves were measured under LI (f=0.0260) at central, intermediate, and corner locations [Fig. 6(b)]. The characteristic worsening of the *I-V* curve at sufficiently high flux (noted in Sec. III A for the uniform grid cell) is also evident here. In Fig. 6(b), note the current drop at intermediate and low voltages, as well as the location dependence of its onset as a function of P_{in}. At the center of the cell, with greatest local metallization, the signature worsening of the *I-V* curve starts only at $P_{in}>4$ W, whereas at the corner of the cell, with least local metallization, the current drop is already apparent at $P_{in}=2$ W. In addition, the decline in cell performance here is observable in both the intermediate *and* low voltage regimes (elaborated in Sec. IV).

Figure 7 shows how V_{oc}, FF, and η depend on flux at different locations. The observed trends will be addressed in Sec. IV, along with the questions of whether (1) these osten-

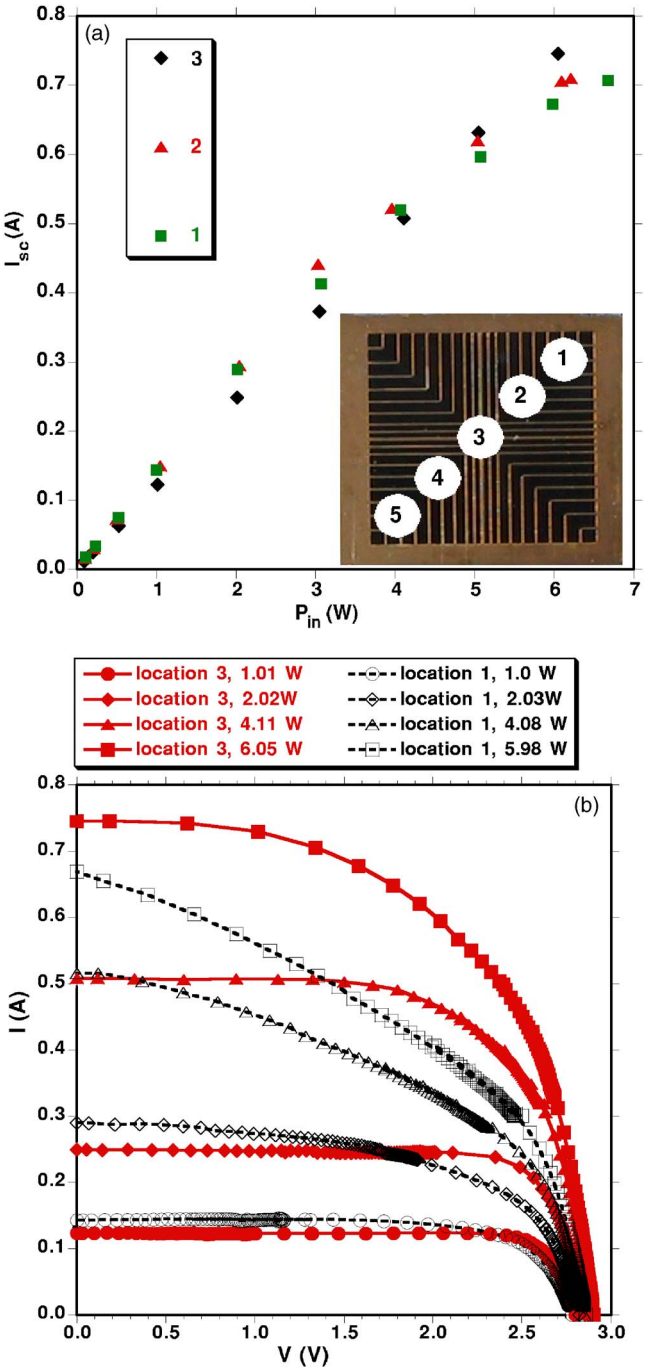

FIG. 6. (Color online) (a) I_{sc} measured at central, intermediate, and corner locations. The inset illustrates locations of the LI spot on the cell surface. Data for points 4 and 5 are not shown because they coincide with those for points 2 and 1, respectively, which reflects the central symmetry. (b) Representative *I-V* curves from LI tests at central and corner locations of the nonuniform grid cell. Data for points 4 and 5 are not shown because they coincide with those for points 2 and 1, respectively, which reflects the central symmetry.

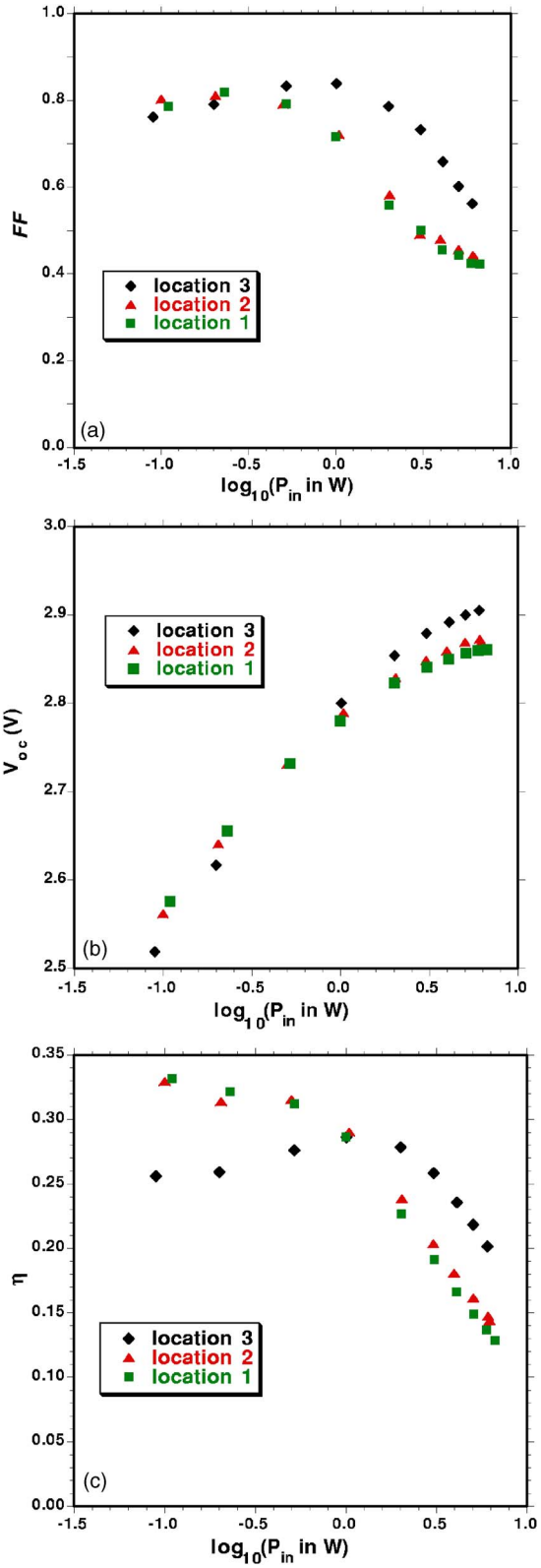

FIG. 7. (Color online) Dependence of FF, V_{oc}, and η on P_{in} and LI location for the *nonuniform* grid cell [locations are identified in Fig. 6(a)].

sibly unusual features are indigenous to high-flux LI tests, (2) there is a relatively simple physical explanation consistent with the observed trends, and (3) the spatial variations in PV parameters can be accounted for from the lateral dependence of series resistance that derives from nonuniform metallization.

IV. INTERPRETATION OF EXPERIMENTAL RESULTS

In this section, our aim is to account for the principal observed trends with a simple model, such that exact determinations of flux-independent lumped series resistance R_s and diode quality factor n are inessential (see the Appendix).

According to the model, the effects of nonuniform illumination should be most pronounced at high P_{in}, high R_s, and small f (more highly localized irradiation), which, together with the realities of high-flux PV systems, motivates parameter selection in the examples that follow. For a uniformly illuminated cell, plots of V_{oc} against $\log(P_{in})$ at constant T are invariably linear [as in the measured upper curve in Fig. 4(a)], independent of R_s, and often used to extract the diode quality factor n and reverse saturation current I_o from the slope and intercept [see Eq. (A2)]. (Small digressions from linearity in the measurements relate to a warming of the cells at the highest P_{in} values due to finite heat rejection rates.) From the data in the low-flux (linear) regime at uniform illumination for the uniform grid cell [Fig. 4(a)], we estimate $n=3.62$ and $I_o=5.2\times10^{-14}$ A (at $T\approx300$ K), which were adopted for all model calculations in Figs. 8–11.

Figure 8(a) illustrates schematically how the model calculation of the I-V curve of the entire cell in LI testing comprises the contributions of the illuminated spot and the remaining dark area. Figure 8(b) provides quantitative examples. Of particular note at adequately high P_{in} is the almost linear I-V behavior between voltages V' and V'' that characterize a particular cell and irradiation pattern. The values of V' and V'' follow from dissipation in the illuminated and dark regions, respectively.

For example, the value of V'', and the rapid decrease in current as V approaches V_{oc}, is imposed by the I_d-V curve for the dark region. Hence the values of V'' and dI/dV at voltages just below V_{oc} should be independent of P_{in}, although strongly affected by R_s and f [see Eqs. (A4)–(A6)]. The I-V curve of the entire cell is dominated by (1) the illuminated sector for $V<V''$ and (2) the dark zone for $V>V''$.

The value of V', however, decreases rapidly as P_{in} is increased and can even reach 0 at large enough P_{in}, as a consequence of significant R_s losses. When $V'=0$, the FF for the illuminated region reaches its minimum of 0.25, but the FF for the entire cell saturates at a value >0.25 - a point to which we shall return shortly. The appearance and slope of the linear region (delimited by V' and V'') follow from the contribution of the illuminated area and are controlled by R_s.

The model indicates that at low flux, V' exceeds V'', which would preclude the appearance of the special I-V features portrayed immediately above [i.e., I-V curves should then be akin to those in Fig. 5(a)]. However, there is a threshold value of P_{in} above which V'' exceeds V', so the I-V characteristic illustrated in Fig. 8 should be observable.

The key trends of the model when series resistance effects are non-negligible [Fig. 8(b)] are in accord with our experimental findings. Consider, for example, the LI I-V measurements summarized in Figs. 5(b) and 6(b). The onset of a nominally linear section accompanies higher P_{in}, with the lower delimiting voltage V' decreasing at larger P_{in}. V' reaches 0 at flux values that are high but realizable in practical concentrators [Fig. 6(b)]. At the same time, V'' is almost independent of P_{in}.

These indicators also provide a comparison between local R_s values in the two classes of cells studied here as follows. The pronounced current drop (at V just above V'') is found experimentally when P_{in} exceeds 5 W for the uniform grid cell [Fig. 5(b)] and 4 W at the center of the cell with irregular metallization [Fig. 6(b)]. But the illuminated fraction f for the uniform grid cell was considerably smaller (0.007 85 vs 0.026). The fact that a lower P_{in} threshold is measured at greater f in the *nonuniform* grid cell indicates R_s at its center is larger than that at the center of the uniform grid cell.

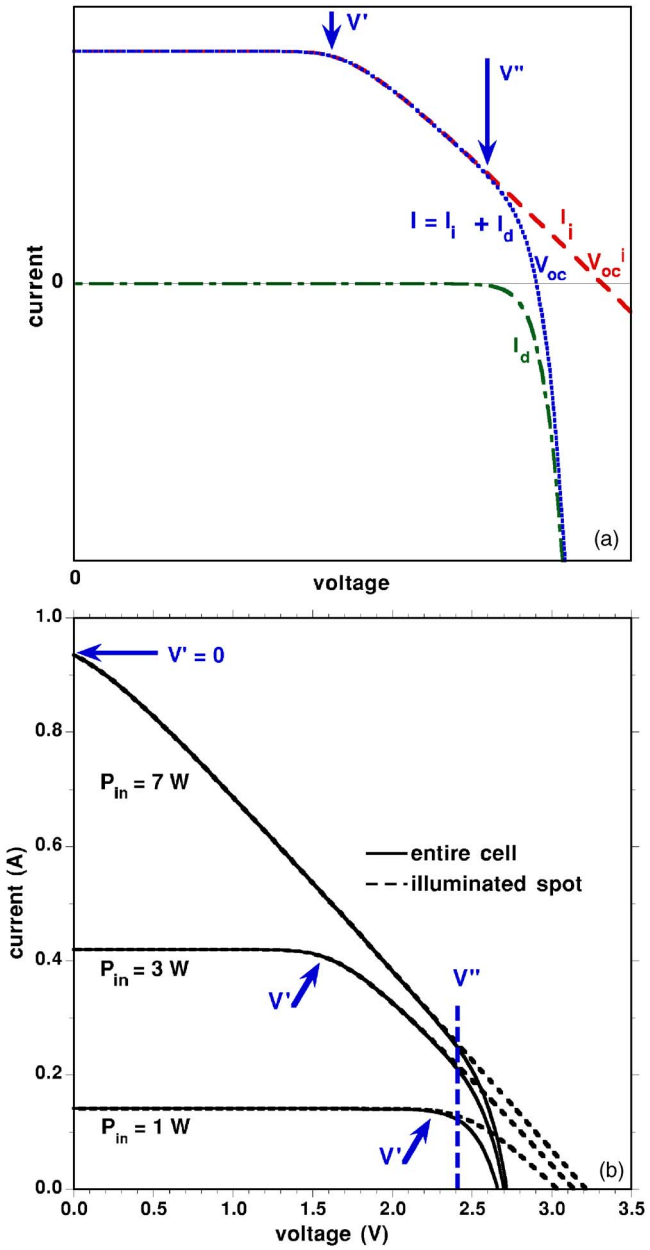

FIG. 8. (Color online) (a) Schematic illustration of how the current-voltage curves of the dark (d) and illuminated (i) regions of a cell under LI combine to yield the measured curve. V_{oc} and V_{oc}^{i} denote the respective open-circuit voltages of the entire cell and the localized illuminated spot. (b) Sample calculated current-voltage curves for the illuminated region and the entire cell, at varying P_{in} with $f=0.0260$ and $R_s=0.080$ Ω.

Next, consider the lateral nonuniformity observed in the P_{in} threshold. At the cell corner, the measured P_{in} threshold is only 2 W [Fig. 5(b)]. In addition, the measured values of V' near the corner are noticeably lower than the corresponding values at the cell's center. In the experiments at $P_{in}\geqslant4$ W, V' has reached 0. These points are accounted for by

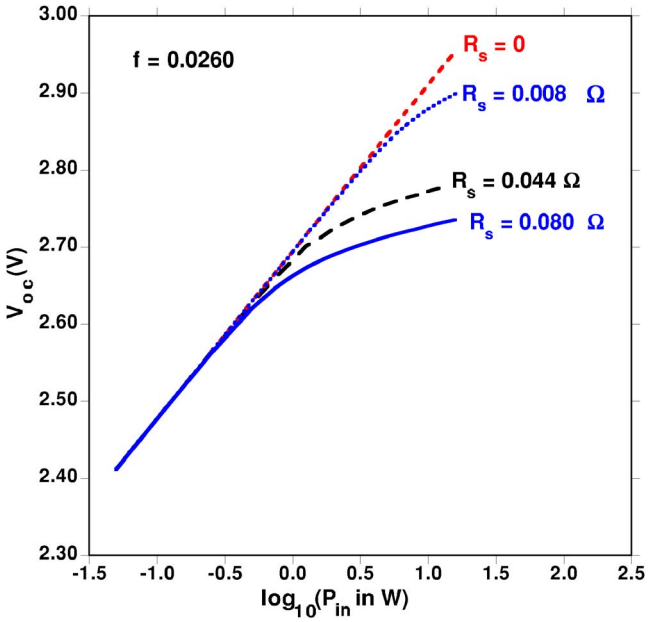

FIG. 9. (Color online) Calculated V_{oc} vs $\log(P_{in})$, illustrating sensitivity to R_s under localized irradiation.

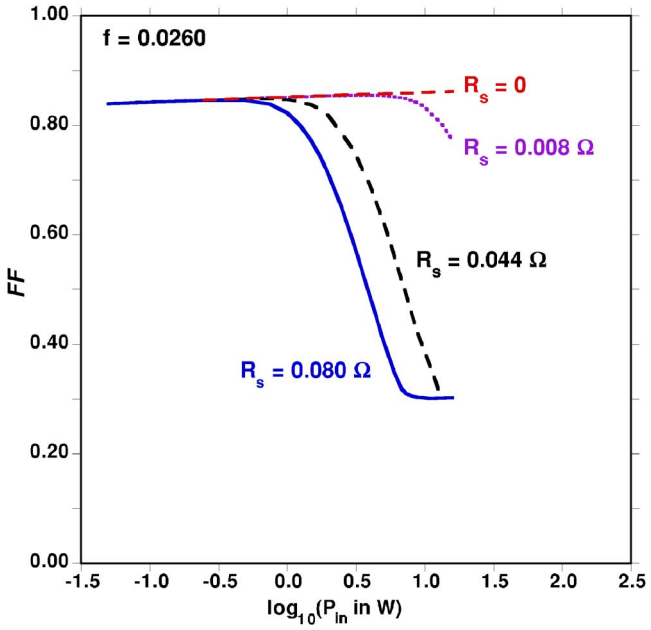

FIG. 10. (Color online) Calculated FF as a function of $\log(P_{in})$ for LI, illustrating sensitivity to R_s.

a model with a local series resistance that increases from the cell center to its corners. Model predictions are also consistent with the nonlinear variation of I_{sc} with P_{in} once P_{in} is sufficiently high that $V'=0$ [e.g., the data for corner point 1 in Fig. 6(a)].

A rigorous analysis of LI experiments requires more sophisticated calculations based on a distributed series resistance[14–16] and, for solar cells with nonuniform metallization, three-dimensional (3D) modeling.[17] For example, being oversimplified, our one-dimensional (1D) model predicts a linear current drop in the intermediate voltage range from V' to V'' whereas some measurements revealed rounded quasilinear *I-V* functions [e.g., data for the uniform grid cell at $P_{in}=5-8$ W in Fig. 5(b), as well as data for the center of the nonuniform grid cell at $P_{in}=4-6$ W in Fig. 6(b)]. A similar type of rounded *I-V* characteristic under similar nonuniform illumination was recently calculated using a proper 3D distributed series resistance model.[18]

Addressing the flux dependence of the principal cell parameters, we note that with localized rather than uniform irradiation, the unequal area weightings [Eqs. (A4)–(A6) in the Appendix] should give rise to a detectable (1) lowering of V_{oc} and (2) dependence of V_{oc} on R_s at high flux values, even at constant T (Fig. 9). Both effects were observed experimentally [Figs. 4(a) and 7(b)]. A more subtle effect is recognizable in cells with a nonuniform metallization grid when R_s varies locally. In agreement with the calculated trend (Fig. 9), the measurements in Fig. 7(b) reveal a reduction of V_{oc} at high flux as the LI spot moves from the cell's center to its corner (i.e., from lower to higher R_s).

Figure 10 illustrates the calculated trends for FF, consistent with the data reported in Figs. 3 and 7(a). The spatial variation of R_s explains the considerable difference in the measured flux dependence of FF at the central and corner sites of the nonuniform grid cell [Fig. 7(a)]. The reduced FF should saturate at a minimum value of 0.25 in *uniformly* irradiated cells at ultrahigh flux. The uneven area weighting in localized irradiation [Eqs. (A1)–(A6) in the Appendix and Fig. 10] foretells that FF should attain a larger asymptotic value at considerably lower flux, specifically, at P_{in} values high enough to generate $V'=0$.

In Fig. 10, the FF of the entire cell saturates at a value above 0.25 (the curves for the highest R_s values). This stems from saturation of the FF of the illuminated subcell at 0.25 [e.g., the curve calculated at $P_{in}=7$ W in Fig. 8(b)]. The point at which I_{sc} should cease to be proportional to P_{in} is precisely the point at which the knee in the *I-V* curve of the entire cell reaches zero voltage [as in Fig. 8(b)]—a prediction borne out by the data from the corner sites of the nonuniform grid cell at $P_{in} \geqslant 6$ W [Figs. 6(a), 6(b), and 7(a)].

Equivalent trends are also evident in cell efficiency (Fig. 11). At lower flux, plots of η vs $\ln(P_{in})$ should be linear with a slope proportional to $GnkT/q$. Higher flux incurs greater parasitic voltage drops IR_s. For LI, the model indicates an efficiency reduction that grows more pronounced and starts at lower P_{in}, as R_s increases and/or f grows smaller. These trends are clear from the data in Fig. 4(b) for the cells with a uniform grid. The interpretation for the cells with a nonuniform grid [Fig. 7(c)] should account for the observations that (1) different LI locations have different local shaded (metallized) fractions and hence different G values and (2) the local R_s at the noncentral sites would appear to be sufficiently large that η starts to decrease at lower flux [Fig. 7(c)].

V. SUMMARY

Interrogating solar cells with localized irradiation offers a nonintrusive tool for establishing PV characteristics and their spatial dependence. Such results are of particular value in the latest generations of ultraefficient cells tailored to high concentration, especially with optical systems that can produce strong flux inhomogeneities on an individual cell. The

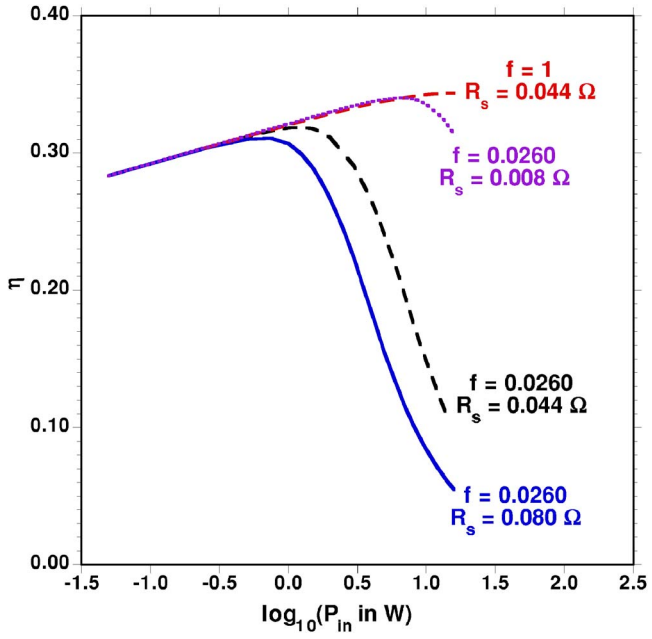

FIG. 11. (Color online) Calculated η as a function of $\log(P_{\text{in}})$, illustrating sensitivity to R_s and f.

LI experimental procedure has been shown to attain local flux levels of 10^4 suns with a circle of concentrated sunlight 1.0 mm in diameter and is applicable to any concentrator solar cell. However, interpretation of the results with detailed PV modeling can vary with cell architecture.

The two case studies presented here address the impact of series resistance and its spatial dependence on cell performance, including the value of a nonuniform metallization grid. The experimental results illustrate the value of the LI technique for identifying inhomogeneities in PV parameters, as well as the effects of light intensity and flux uniformity. Several features uncommon to earlier reports of PV *I-V* curves, and of the flux dependence of fundamental PV parameters such as FF, I_{sc}, V_{oc}, and η, have been identified, and the trends have been accounted for with a simple physical model.

ACKNOWLEDGMENTS

One of the authors (E.A.K.) thanks the Israel Ministry of Immigrant Absorption and the Deichmann Foundation for financial support.

APPENDIX: 1D EQUIVALENT CIRCUIT MODEL FOR INTERPRETING THE EXPERIMENTAL RESULTS

1. Uniform irradiation

We adopt a standard 1D equivalent circuit,[19]

$$I = I_p - I_o\left[\exp\left(\frac{q(V+IR_s)}{nkT}\right) - 1\right] \text{ or, explicitly}$$

$$V = \frac{nkT}{q}\ln\left(1 + \frac{I_p - I}{I_o}\right) - IR_s, \tag{A1}$$

where I_p is the photogenerated current (strictly proportional to P_{in}, I_o is the reverse saturation current, T is cell temperature, k is Boltzmann's constant, and q is the magnitude of electron charge. [Shunt losses are negligible, attested to by the essentially horizontal *I-V* curves in the low-voltage regime of Figs. 5 and 6(b) when flux levels are low enough that significant R_s losses are not incurred.]

For a given *I-V* trace, I_p is constant and the voltage dependence originates from the dark (diode) current contribution, including R_s losses. For example, as R_s increases, the dark current achieves a significant magnitude at progressively lower voltage, and the sharp "knee" of the *I-V* curve (high FF) softens as FF lessens. I_{sc} and V_{oc} remain unchanged,

$$V_{\text{oc}} = \frac{nkT}{q}\ln\left[\frac{I_p}{I_o} + 1\right] \approx \frac{nkT}{q}\ln\left[\frac{I_p}{I_o}\right], \tag{A2}$$

$$I_{\text{sc}} = I_p - I_o\left[\exp\left(\frac{qI_{\text{sc}}R_s}{nkT}\right) - 1\right]$$

$$\approx I_p \quad \text{(except at very high flux or } R_s\text{)}. \tag{A3}$$

With $I_p \propto P_{\text{in}}$, plots of V_{oc} against $\log(P_{\text{in}})$, and I_{sc} against P_{in} should be strictly linear.

For a cell of given R_s, the *I-V* curve in this model worsens as P_{in} is increased due to enhanced series resistance losses. At low flux, this decline is observed only at high voltage (near V_{oc}). It expands to lower voltages as P_{in} increases. Eventually, the knee reaches zero voltage, and the *I-V* curve becomes a straight line, for which FF reaches its minimum value of 0.25. Further increasing P_{in} does not alter FF but lowers I_{sc}. For high-quality concentrator cells of the type studied here (with low R_s), the FF saturation effect may be detectable only at ultrahigh flux beyond anticipated operating conditions.

2. Localized irradiation

These trends change when the light is localized. The photogeneration and dissipative resistive contributions are no longer weighted by the same area [in Eq. (A1)]. For simplicity, the entire cell can be viewed as the parallel connection of uniformly illuminated (i) and dark (d) subcells

$$I = I_i + I_d. \tag{A4}$$

If the resistive contribution of the metallization is negligible relative to the other factors comprising R_s, then R_s can be approximated as the ratio of a constant specific series resistance to subcell area:[11]

$$I_d = -I_o(1-f)\left[\exp\left(\frac{q[V + I_dR_s/(1-f)]}{nkT}\right) - 1\right], \tag{A5}$$

$$I_i = I_{\text{sc}} - I_o f\left[\exp\left(\frac{q(V + I_iR_s/f)}{nkT}\right) - \exp\left(\frac{qI_{\text{sc}}R_s}{nkTf}\right)\right], \tag{A6}$$

where both zones are assumed to have the same n, I_o, and T.

[1] M. Yamaguchi, T. Takamoto, K. Araki, and N. Ekins-Daukes, Sol. Energy **79**, 78 (2005).
[2] R. R. King *et al.*, International Conference on Solar Concentrators for the Generation of Electricity or Hydrogen, Scottsdale, AZ, May 2005, National Renewal Energy Laboratory, Golden, CO, NREL/CD-520-38172;

G. Glenn and R. Sherif (private communication), Spectrolab Corp., Sylmar, CA.
[3]F. Dimroth, R. Beckert, M. Meusel, U. Schubert, and A. W. Bett, Prog. Photovoltaics **9**, 165 (2001).
[4]D. Feuermann, J. M. Gordon, S. Horne, G. Conley, and R. Winston, Proc. SPIE **5942**, 250 (2005).
[5]R. Winston and J. M. Gordon, Opt. Lett. **30**, 2617 (2005).
[6]R. Winston, J. C. Miñano, and P. Benítez, *Nonimaging Optics* (Elsevier, Oxford, 2005).
[7]J. M. Gordon, E. A. Katz, D. Feuermann, and M. Huleihil, Appl. Phys. Lett. **84**, 3642 (2004).
[8]J. M. Gordon, E. A. Katz, W. Tassew, and D. Feuermann, Appl. Phys. Lett. **86**, 073508 (2005).
[9]E. A. Katz, J. M. Gordon, and D. Feuermann, Prog. Photovoltaics **14**, 297 (2006).
[10]Under LI conditions, the resistance of the uniform metallization [Fig. 2(a)] approximately comprises the parallel connection of two resistances rx and $r(L-x)$, where r is the specific resistance per unit length of contact fingers, x is the distance between the LI location and one of the busbars, and L is the distance between the busbars. This resistance is greatest at the cell's center and smallest near the busbars. If the metallization contributes non-negligibly to R_s, then a lateral dependence to FF should be observed.
[11]A. Luque, *Solar Cells and Optics for Photovoltaic Concentration* (IOP, Bristol, 1989), Chap. 4, pp. 103–135.
[12]C. Algora and V. Diaz, Prog. Photovoltaics **8**, 211 (2000).
[13]K. Nishioka, T. Takamoto, T. Agui, M. Kaneiwa, Y. Uraoka, and T. Fuyuki, Sol. Energy Mater. Sol. Cells **90**, 1308 (2006).
[14]G. M. Smirnov and J. E. Mahan, Solid-State Electron. **23**, 1055 (1980).
[15]L. D. Nielsen, IEEE Trans. Electron Devices **ED-29**, 821 (1982).
[16]V. M. Andreev, V. A. Grilikhes, and V. D. Rumyantev, *Photovoltaic Conversion of Concentrated Sunlight* (Wiley, Chichester, 1997).
[17]B. Galiana, C. Algora, I. Rey-Solle, and I. G. Vara, IEEE Trans. Electron Devices **52**, 2552 (2005).
[18]P. Benítez and J. C. Miñano, in *Next Generation Photovoltaics*, edited by A. Marti and A. Luque (IOP, Bristol, 2004) Chap. 13.
[19]M. Green, *Solar Cells* (University of New South Wales, Kensington, 1986), pp. 76–79.